JOURNAL OF MATERIALS SCIENCE **34** (1999) 6165–6168

Effects of binary additives B_2O_3-Y_2O_3 on the microstructure and thermal conductivity of aluminum nitride ceramics

HEPING ZHOU, YAOCHENG LIU, WEIGUO MIAO, YIN WU
State Key Laboratory of New Ceramics and Fine Processing, Department of Materials Science and Engineering, Tsinghua University, Beijing 100084, People's Republic of China
E-mail: zhp-dms@mail.tsinghua.edu.cn

Aluminum nitride (AlN) ceramics, with binary additives B_2O_3-Y_2O_3, were sintered at temperatures from 1700 to 1850 °C. The microstructure and sintering characteristics were studied by XRD, HREM, SEM and TEM/EDS, which showed that Y_2O_3 gave different yttrium aluminates through the reaction with Al_2O_3 under different conditions. With the increase of sintering temperature, the yttrium-to-aluminum atomic ratio Y/Al decreased in the secondary phases of the sintered bodies. It was discovered that B_2O_3 could dissolve in the yttrium aluminates, forming some ordered structure with a superlattice. After sintering at 1850 °C for 4 h, a specimen with a fine microstructure and a thermal conductivity of 190 $W\,m^{-1}\,K^{-1}$ was obtained.

1. Introduction

Aluminum nitride (AlN) has been intensely studied for electronic ceramic packaging due to its remarkable properties such as high thermal conductivity, low dielectric constant, a thermal expansion coefficient matching that of silicon, and a nontoxic nature [1, 2]. However, as oxygen impurity can easily dissolve into AlN lattice, generating aluminum vacancies which scatter phonons, AlN can hardly get its intrinsic thermal conductivity, 319 $W\,m^{-1}\,K^{-1}$ [3, 4]. With the increase of oxygen content, the thermal conductivity of AlN heavily deteriorates. On the other hand, being mainly a covalent bond crystal, AlN is difficult to sinter. People used Y_2O_3, CaO and other compounds as sintering aids [5, 6, 7]. Because Y_2O_3 can yield yttrium aluminates through the reaction with Al_2O_3, which removes the dissolved oxygen in AlN lattice, it is beneficial to the thermal conductivity of AlN ceramics. Virkar [8] explained the variation in thermal conductivity with the type and the amount of the additive on the basis of the thermodynamics of oxygen removal and proposed that the higher the $|\Delta G^\circ|$, with $\Delta G^\circ < 0$, ΔG° being the formation free energy of aluminates, the higher is the resultant thermal conductivity. It is of great importance to choose appropriate sintering aids to lower the sintering temperature and improve the thermal conductivity of AlN ceramics.

In the present study, AlN ceramics were sintered at different temperatures, using the binary system of B_2O_3-Y_2O_3 as additives. The produced phases and microstructural characteristics of as sintered specimens were investigated through X-ray diffraction (XRD), high-resolution electron microscope (HREM), scanning electron microscope (SEM) and transmission electron microscope together with energy dispersive spectrometer (TEM/EDS). The relation between thermal conductivity and microstructure is discussed.

2. Experimental

2.1. Specimen preparation

Commercial AlN powder with 1.0 wt % of oxygen and an average particle size of 2.7 μm was used as raw material, doped with 2.4 wt % of B_2O_3 and 1.6 wt % of Y_2O_3. The powders were mixed by ball milling for 48 h, with alcohol as the medium. After being dried, they were placed into graphite crucible, embeded with AlN powder, and pressurelessly sintered at 1700 °C (specimen A1), 1750 °C (specimen A2), 1800 °C (specimen A3) and 1850 °C (specimen A4) for 4 h respectively, with a flowing nitrogen atmosphere.

2.2. Characterization

Densities of the sintered specimens were measured with Archimedes method. Their thermal conductivities were examined by an ac calorimetric method [9]. XRD was used to identify the contained phases and measure the lattice parameters of them. HREM, SEM and TEM/EDS were employed in the microstructural observation.

3. Results

3.1. Thermal conductivities

Fig. 1 gives the densities and thermal conductivites of specimens sintered at different temperatures. As it shows, with the increase of sintering temperature, the thermal conductivity keeps increasing linearly and monotonously but the density stops increasing at about 1800 °C, when it reaches a value of 3.25 $g\,cm^{-3}$.

TABLE I Secondary phases in specimens sintered at different temperatures

Specimen	Sintering temperature (°C)	Secondary phases
A1	1700	$Al_9N_7O_3$, $Y_4Al_2O_9$
A2	1750	$Y_4Al_2O_9$, $YAlO_3$
A3	1800	$YAlO_3$, $Y_3Al_5O_{12}$
A4	1850	$YAlO_3$, $Y_3Al_5O_{12}$

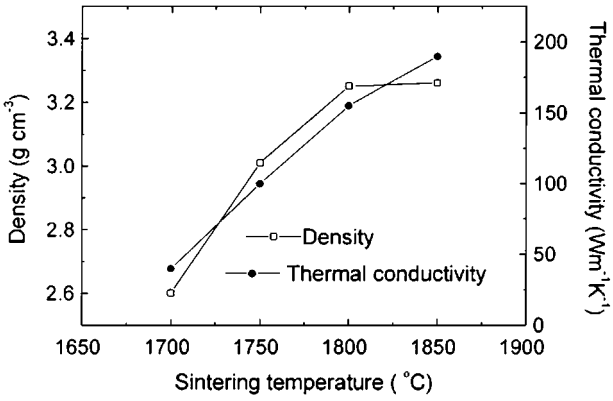

Figure 1 Dependence of density and thermal conductivity on sintering temperature for AlN doped with B_2O_3-Y_2O_3.

3.2. XRD and HREM analysis

Table I displays the phases identified by XRD in different specimens, which indicates that by sintering at different temperatures, the contained phases had different types and amounts.

In specimen A1, due to the relatively low sintering temperature (1700 °C), the dissolved oxygen in AlN lattice could not fully diffuse to the grain boundary, therefore existed the aluminum oxynitride phase, $Al_9N_7O_3$. With an increase of the sintering temperature, more oxygen impurities were transported to the grain boundaries to react with Y_2O_3, forming yttrium aluminates with a smaller yttrium-to-aluminum atomic ratio Y/Al. Consider the following reactions:

$$3Y_2O_3 + 5Al_2O_3 \rightarrow 2Y_3Al_5O_{12} \quad \text{(i)}$$

$$5Y_2O_3 + 5Al_2O_3 \rightarrow 10YAlO_3 \quad \text{(ii)}$$

$$10Y_2O_3 + 5Al_2O_3 \rightarrow 5Y_4Al_2O_9 \quad \text{(iii)}$$

$$2Y_3Al_5O_{12} + 2Y_2O_3 \rightarrow 10YAlO_3 \quad \text{(iv)}$$

$$10YAlO_3 + 5Y_2O_3 \rightarrow 5Y_4Al_2O_9 \quad \text{(v)}$$

Note that reaction (ii) is the sum of reactions (i) and (iv), reaction (iii) is the sum of reactions (ii) and (v). Thus, $\Delta G^\circ_{ii} = \Delta G^\circ_i + \Delta G^\circ_{iv}$, $\Delta G^\circ_{iii} = \Delta G^\circ_{ii} + \Delta G^\circ_v$. Clearly, all of the ΔG° values are less than zero because these reactions do occur. Hence, $\Delta G^\circ_{iii} < \Delta G^\circ_{ii} < \Delta G^\circ_i < 0$ [8]. During sintering, $Y_4Al_2O_9$ was first generated. When the temperature became high enough, the major secondary phases were $YAlO_3$ and $Y_3Al_5O_{12}$.

By HREM, defects in the AlN lattice could be easily observed in specimen A1, like those displayed in Fig. 2. While in specimen A4, the lattice was found to be perfect, with few defects. This partially explains the difference between the thermal conductivities of specimens sintered at different temperatures.

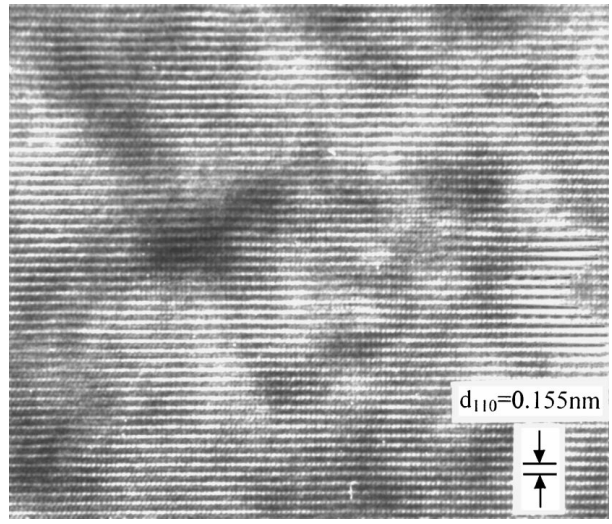

Figure 2 HREM photograph of specimen A1.

The measurement of the lattice parameters revealed that the lattice parameters of AlN in the sintered bodies were almost the same as those of pure AlN, while there were small changes in the parameters of the yttrium aluminates. In specimen A4, the experimental values of *a* were 11.9828 and 12.042 Å for $Y_3Al_5O_{12}$ and $YAlO_3$, respectively, less than the standard values, 12.0089 and 12.107 Å. It was supposed that B_2O_3 dissolved into the yttrium aluminates, forming $Y(Al_{1-x}B_x)O_3$ and $Y_3(Al_{1-x}B_x)_5O_{12}$ solid solutions. As the radius of B^{3+} is just 0.23 Å, much smaller than that of Al^{3+}, 0.53 Å [10], the lattice parameters of yttrium aluminates were led to decline. This will be further discussed in Section 3.3.

3.3. SEM and TEM/EDS investigation

The SEM observation showed that when the sintering temperature rose, the AlN grain size increased, with less porosity and a smaller volume of grain-boundary phases. In the 1800 °C sintered specimen, the grains have fully grown, taking polyhedral configurations (Fig. 3).

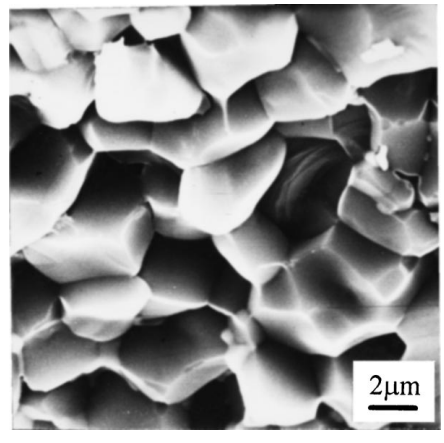

Figure 3 SEM fractograph of specimen A3.

The microstructure can be studied more clearly by TEM/EDS. In specimens sintered at relatively low temperatures, the secondary phases are distributed not only at the triple-grain junctions, but also along the edges of AlN grains, with considerable thickness. In those sintered at higher temperatures, the secondary phases mainly existed at the triple-grain junctions, with straight narrow grain boundaries. The EDS and electron diffraction patterns indicated the secondary phases to be crystalline yttrium aluminates.

The diffraction patterns showed that in specimen A4, the secondary phase at the triple-grain junction was yttrium aluminum garnet (YAG), with some ordered structure of superlattice. The YAG has a cubic structure, with $a = 12.0089$ Å and a space group of I$a3d$. Consider the formula of YAG, $Y_3Al_2(AlO_4)_3$ [11]. In each unit cell, eight formulae of $Y_3Al_2(AlO_4)_3$ are included, with 16 Al^{3+} occupying the *a* positions, which are the interstices of oxygen octahedrons, 24 Al^{3+} at the *d* positions, the interstices of oxygen tetrahedrons. Due to the low atomic number of boron, it could not be detected by EDS, even though it dissolved into $Y_3Al_5O_{12}$. As the radius of B^{3+} is small, when entering the $Y_3Al_2(AlO_4)_3$ lattice, it should occupy the *d* position. If an ordered structure was formed through some process, the formula might be $Y_3Al_2(Al_{0.5}B_{0.5}O_4)_3$. Fig. 4 exhibits the assumed arrangement of Al^{3+} and B^{3+} on (001) plane.

To confirm this assumption, we calculated the relative diffraction intensities of this structure. Table II lists the results, as well as the data of $Y_3Al_2(AlO_4)_3$ given by powder diffraction file (PDF). For $Y_3Al_2(AlO_4)_3$, the intensity of (110) plane is zero. While for $Y_3Al_2(Al_{0.5}B_{0.5}O_4)_3$, as the ordered structure was formed, (110) plane had a certain diffraction intensity, which agreed with the electron diffraction patterns.

TABLE II Calculated diffraction intensities of $Y_3Al_2(AlO_4)_3$ and $Y_3Al_2(Al_{0.5}B_{0.5}O_4)_3$

	$Y_3Al_2(AlO_4)_3$			$Y_3Al_2(Al_{0.5}B_{0.5}O_4)_3$	
(*h k l*)	I/I_0 (PDF 33-40)	I	I/I_0	I	I/I_0
110	0	0	0	1.88	4
211	27	23.9	39	32.0	64
220	7	5.54	9	3.58	7
321	19	12.2	20	17.2	34
400	27	14.4	24	12.9	26
420	100	61.2	100	50.1	100
422	20	12.9	21	10.7	21
431	6	3.00	5	5.81	12
521	23	14.2	23	13.0	26
440	5	3.20	5	2.57	5

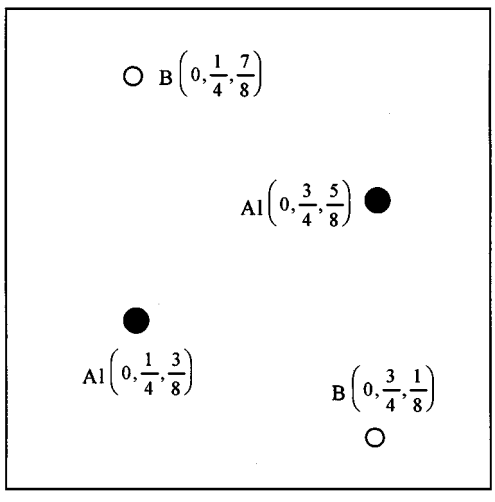

Figure 4 Arrangement of atoms on (001) plane for $Y_3Al_2(Al_{0.5}B_{0.5}O_4)_3$ with ordered structure.

4. Discussion

In order to improve the thermal conductivity of AlN ceramics, several considerations are important. (i) Full densification should be obtained, with lowest porosity. (ii) Oxygen impurities should be successfully removed from the AlN lattice. (iii) Fine microstructure should be achieved, with least grain boundary phases and close contact between grains.

According to the phase diagram [12], a liquid phase can be obtained at about 1400 °C in the B_2O_3-Y_2O_3 system, in which Al_2O_3 can be effectively dissolved. With the raise of sintering temperature, the liquid volume increases, and the solubility of Al_2O_3 also increases, which enhance the growth of AlN grains and the removal of oxygen resulted defects. The dominant densification mechanism is solution-precipitation. The 1750 °C sintered specimen got a density of 3.01 g cm^{-3}, and a thermal conductivity of 100 W m^{-1} K^{-1}.

The doped Y_2O_3 could react with Al_2O_3 on the surface of AlN particles, generating yttrium aluminates at the grain boundaries thus lower the oxygen content in the AlN grains and improve the thermal conductivity of AlN ceramics. As the sintering temperature increased, the yttrium-to-aluminum atomic ratio of the generated yttrium aluminates declined, inferring that more Al_2O_3 had been absorbed into the grain boundary phase.

As a sintering aid, B_2O_3, together with Y_2O_3 and Al_2O_3, resulted in an eutectic reaction at quite a low temperature, forming a liquid phase and enhancing densification. In specimens sintered at temperatures lower than 1750 °C, the glassy layers were found between AlN grains by SEM. When heated to a higher temperature, B_2O_3 dissolved into the lattice of yttrium aluminates, which led to the crystallization and contraction of liquid phase, cleaning the grain boundaries.

When the sintering temperature was raised to higher than 1800 °C, the thermal conductivity prominently increased although the density barely grew. This can be explained by the microstructural changes during sintering. At a higher temperature, the transportation of oxygen from AlN grains to grain boundaries became easier and quicker. For a same soaking time, the oxygen resulted defects could be more fully removed if sintered at higher temperature. On the other hand, the growth of AlN grains was promoted as temperature rose, which drove the liquid phase to the triple-grain junctions, therefore made the grains contact with each other face to face and enlarged the heat diffusion cross-section. After sintering at 1850 °C for 4 h, specimen A4 had a thermal conductivity of 189 W m^{-1} K^{-1}.

5. Conclusion

In sintering AlN ceramics with B_2O_3-Y_2O_3 binary additives, the transport mechanism was solution-precipitation. When raising the sintering temperature, the density increased, AlN grains grew to perfect configuration, with less amount of secondary phase, the Y/Al ratio of the produced yttrium aluminates declined. It was found that B_2O_3 was an effective sintering additive in assisting densification. At high temperature, B^{3+} dissolved into the yttrium aluminates, partially displacing Al^{3+}. By this the ordered structures with superlattices were formed. The B_2O_3-Y_2O_3 doped AlN ceramics reached a thermal conductivity of 190 $W\,m^{-1}\,K^{-1}$ after sintering at 1850 °C for 4 h.

Acknowledgements

This work was supported by National Natural Science Foundation of China.

References

1. R. R. TUMMALA, *J. Amer. Ceram. Soc*. **74** (1991) 895.
2. USACA, *Amer. Ceram. Soc. Bull*. **69** (1990) 1804.
3. G. A. SLACK, *J. Phys. Chem. Solids* **34** (1973) 521.
4. G. A. SLACK, R. A. TANZILLI, R. O. POHL and J. W. VANDERASNDE, *ibid.* **48** (1987) 641.
5. K. KOMEYA, H. INOUE and A. TSUGE, *J. Amer. Ceram. Soc*. **57** (1974) 411.
6. P. S. DE BARANDA, A K. KNUDSEN and E. RUH, *ibid*. **76** (1993) 1751.
7. K. WATARI, A. TSUZUKI and Y. TORII, *J. Mater. Sci. Lett.* **11** (1992) 1508.
8. A. V. VIRKAR, T. B. JACKSON and R. A. CUTLER, *J. Amer. Ceram. Soc*. **72** (1989) 2031.
9. I. HATTA, Y. SASUGA, R. KATO and A. MAESONO, *Rev. Sci. Instrum.* **56** (1985) 1643.
10. R. D. SHANNON and C. T. PREWITT, *Acta Cryst.* **B25** (1969) 925.
11. E. PRINCE, *ibid.* **10** (1957) 787.
12. E. M. LEVIN and H. F. MCMURDIE, "Phase Diagrams for Ceramists" (*Amer. Ceram. Soc*., Columbus, 1975) p. 140.

Received 3 February 1998
and accepted 5 May 1999